

# Using Multi-Instance Learning to Identify Unique Polyps in Colon Capsule Endoscopy Images

Puneet Sharma<sup>1\*</sup>, Kristian Dalsbø Hindberg<sup>2</sup>, Eibe Frank<sup>3</sup>,  
Benedicte Schelde-Olesen<sup>4,5</sup>, Ulrik Deding<sup>4,5</sup>

<sup>1</sup>\*Department of Automation and Process Engineering, Machine Learning Group, UiT – The Arctic University of Norway, Tromsø, Norway.

<sup>2</sup>Department of Physics and Technology, Machine Learning Group, UiT – The Arctic University of Norway, Tromsø, Norway.

<sup>3</sup>Department of Computer Science, University of Waikato, Hamilton, New Zealand.

<sup>4</sup>Department of Surgery, Odense University Hospital, Odense, Denmark.

<sup>5</sup>Department of Clinical Research, University of Southern Denmark, Odense, Denmark.

\*Corresponding author(s). E-mail(s): [puneet.sharma@uit.no](mailto:puneet.sharma@uit.no);

Contributing authors: [kristian.d.hindberg@uit.no](mailto:kristian.d.hindberg@uit.no);  
[eibe.frank@waikato.ac.nz](mailto:eibe.frank@waikato.ac.nz); [benedicte.schelde-olesen@rsyd.dk](mailto:benedicte.schelde-olesen@rsyd.dk);  
[ulrik.deding@rsyd.dk](mailto:ulrik.deding@rsyd.dk);

## Abstract

Identifying unique polyps in colon capsule endoscopy (CCE) images is a critical yet challenging task for medical personnel due to the large volume of images, the cognitive load it creates for clinicians, and the ambiguity in labeling specific frames. This paper formulates this problem as a multi-instance learning (MIL) task, where a query polyp image is compared with a target bag of images to determine uniqueness. We employ a multi-instance verification (MIV) framework that incorporates attention mechanisms, such as variance-excited multi-head attention (VEMA) and distance-based attention (DBA), to enhance the model's ability to extract meaningful representations. Additionally, we investigate the impact of self-supervised learning using SimCLR to generate robust embeddings. Experimental results on a dataset of 1912 polyps from 754 patients demonstrate that attention mechanisms significantly improve performance, with DBA L1 achieving the highest test accuracy of 86.26% and a test AUC of 0.928 using a ConvNeXt

backbone with SimCLR pretraining. This study underscores the potential of MIL and self-supervised learning in advancing automated analysis of Colon Capsule Endoscopy images, with implications for broader medical imaging applications.

**Keywords:** multi-instance learning, colon capsule endoscopy, deep learning, polyps

## 1 Introduction

The multiple instance problem (MIP) occurs when the training examples are ambiguous [1]. In such cases, a single example object can be represented by multiple alternative feature vectors (instances), and it is unclear which of the feature vectors are responsible for the object’s observed classification [1].

Multiple instance learning (MIL) builds on the concept of MIP and is a type of machine learning framework where each training example is represented as a bag containing multiple instances, rather than a single feature vector [2, 3]. In this framework, the label is assigned to the entire bag, not to individual instances. The goal of multi-instance learning is to predict the label of unseen (both positive and negative) bags by analyzing the instances within them [2, 3].

In this paper, we apply a recently introduced variant of MIL called multi-instance verification (MIV) [4]. In MIV, a training example consists of a bag of instances *plus* a single query instance. Such a training example is labeled positive if the query instance matches some instances in the target bag and negative otherwise. In the application considered in this paper, this is useful because it allows matching a query image against a bag of images when only some of the images in the bag show a clear relationship to the query—even a single clear match should suffice.

Colon capsule endoscopy (CCE) is a non-invasive diagnostic procedure used to examine the colon for abnormalities, such as polyps, inflammation, or signs of colorectal cancer [5–7]. It involves swallowing a small, pill-sized capsule (PillCam COLON 2 from Medtronic or similar from other companies) equipped with a tiny camera, light source, and transmitter [6, 8, 9]. As the capsule travels through the digestive tract, it captures thousands of images of the colon, which are transmitted to an external recording device for subsequent analysis. CCE achieves polyp detection rates comparable to those of optical colonoscopy while also offering enhanced cost-effectiveness [7, 10], and hence is a suitable candidate for colorectal screening. The cost-effectiveness of the CCE approach stems from the overall gains achieved throughout the pipeline, particularly in scenarios where clinicians are involved and patients from remote locations are required to travel to a healthcare facility. By minimizing the need for travel, the approach significantly reduces associated expenses such as transportation, accommodation, and time lost from work for patients. This not only alleviates the financial burden on patients, but also optimizes resource allocation for healthcare providers.

In CCE, a single video fragment corresponding to a particular polyp yields an image sequence (bag) that contains multiple frames (instances). The question we consider in this paper is whether a given other frame extracted from the original video, the query instance, can be successfully matched with the bag if it shows the same polyp as the

images in the bag. Conversely, machine learning should reject a match if the query image does not pertain to the same polyp. This is a good fit for the MIV paradigm because not all frames will necessarily show a clear view of the relevant polyp. In the training data, the label for a particular query-bag pair depends on which specific frames (instances) are clearly associated with the polyp concerned and thus can be matched with the query. MIV helps to handle this ambiguity by focusing on identifying the instances within the bag that match the query best.

It is important to note that as the colon capsule can move back and forth inside the colon, this can result in hundreds of detections of polyps at the end of a CCE and comparing individual images for uniqueness can be a time consuming task, which can be mitigated by using MIL. For instance, if we assume  $N$  polyp detections obtained at the end of a screening, then comparing  $N$  images for uniqueness requires comparing each image with every other image with the number of comparisons  $N(N-1)/2$  and computational complexity of  $O(N^2)$ . By employing MIV and dividing the images into bags, one query image can be compared against multiple ( $k$ ) target images simultaneously. In this manner, With careful bag organization, the number of required comparisons can be reduced to approximately  $N(N-1)/(2k)$ , achieving a computational gain of up to  $k \times$  compared to exhaustive pairwise comparison.

MIL is applied in a large number of medical applications [11] ranging from diabetic retinopathy in retinal images [12], cancer types in stomach computed tomography (CT) images [13], to histology images [14]. In this context, the application of MIL to CCE images is a relatively new direction, and the application of the MIV variant to medical imagery is also novel.

The key contributions of this paper lie in addressing the challenging task of identifying unique polyps in CCE images by formulating it as a MIL problem. The study leverages a MIV framework that uses advanced attention mechanisms, to enhance the model's ability to derive significant representations from ambiguous and complex image data. Furthermore, the paper explores the integration of self-supervised learning through SimCLR to generate robust embeddings, which significantly improve the performance of the MIV framework.

The rest of the paper is organized as follows: Section 2 describes the dataset used in this study, including its structure, characteristics, and the preprocessing steps undertaken to prepare it for analysis. Section 3 outlines the methodology, detailing the MIV framework, the attention mechanisms employed, and the integration of self-supervised learning using SimCLR. Section 4 presents the experimental results, including performance comparisons across different models and attention mechanisms, as well as an analysis of the impact of SimCLR pretraining. In addition, we discuss the challenges encountered and explore the broader implications of the proposed approach. Finally, we conclude the paper by summarizing the key contributions.

## 2 Data

The data used in our study is based on the CareForColon2015 [15, 16] trial conducted in the Danish colorectal cancer screening programme, which used the PillCam™ Colon 2 (Medtronic, USA) [17] camera capsule. We have access to 2,780 polyps from 853

patients from the CareForColon2015 study for which clinicians from the Department of Surgery of Odense University Hospital have exported up to five images per polyp. These five images correspond to 1) first partial, 2) first full, 3) best full, 4) last full, and 5) last partial image of the same polyp. This means that image 1 and 5 might just partially show the polyp. These are images from the same passing, so we know that there are no cases of the same polyp being seen at a significant later passage time. When we restrict the set to those polyps that the clinicians were able to export all these five images, we end up with 1912 polyps from 754 patients. These include 263 patients with one polyp, 204 patients with 2 polyps, 113 patients with 3 polyps, 77 patients with 4 polyps, and the rest with 5 or more polyps. Each set of five images from a polyp is given a unique patient ID and a unique polyp number.

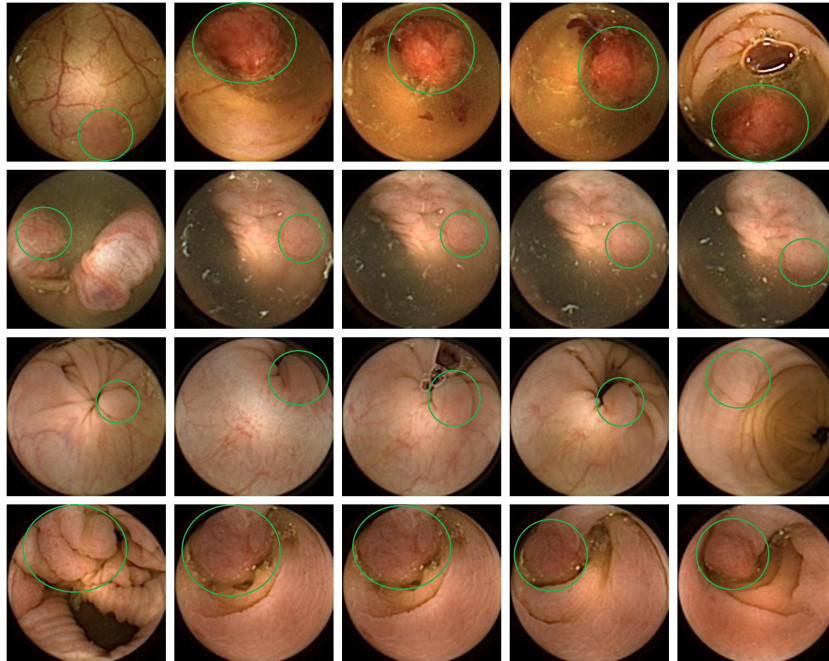


**Fig. 1** Positive exemplar images with each row showing five images of a unique polyp, where in each row, the first image corresponds to first partial and fifth image is the last full view of the same polyp. The polyps have been marked in green for each image.

For MIV, we construct both positive and negative exemplar pairs from this multi-patient polyp image dataset. Positive exemplars are constructed based on the five images from a single polyp, with one of the second, third, or fourth image designated as the query and the remaining four images forming the target bag. Images from five example polyps are shown in Figure 1. Negative exemplars are constructed using a more sophisticated strategy: if a patient has multiple polyps, the query image is selected from one of those polyps at random, while target images are sampled from

other polyps of the same patient; if a patient has only one polyp, target images are drawn from different patients entirely.

To ensure robust evaluation and prevent patient-level data leakage, we implement a patient-level stratification across all data splits. The dataset is first divided into test and training/validation sets at the patient level, with 20% of unique patients reserved for testing. The remaining patients are then partitioned into  $k$ -fold cross-validation splits ( $k=10$ ), where each fold maintains complete patient separation: no patient appears in both training and validation sets of the same fold, and test patients are excluded from all folds entirely. This stratification strategy ensures that the model's generalization is evaluated on genuinely unseen patients providing a more realistic assessment of clinical deployment performance.

### 3 Method

In this section, we briefly discuss the details of the MIV approach and the MIV with SimCLR approach used for our experiments.

#### 3.1 Multi-instance Verification

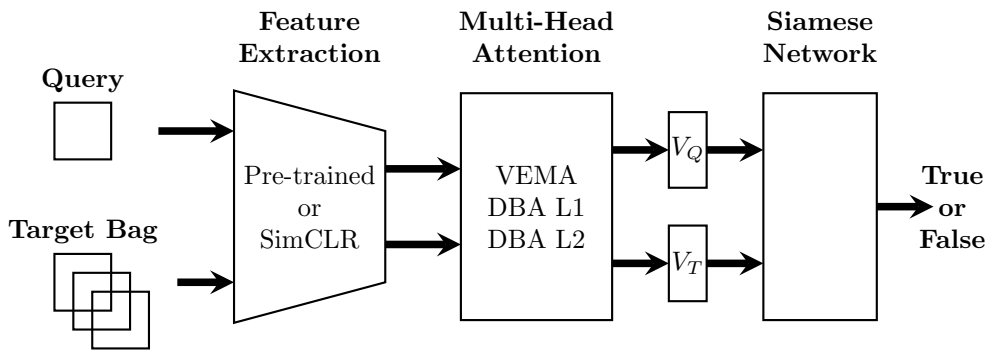


**Fig. 2** A diagram showing the framework used for MIV in this study. The feature extraction is performed for both the query image and the target bag. Multi-head attention mechanisms are used to extract representations from the query, denoted by  $V_Q$ , and the target set, denoted by  $V_T$ . These representations are then used by a Siamese network for the classification task.

For our implementation, we use a Siamese neural network designed for MIV, based on [4]. The network consists of a shared feature transformation that projects input embeddings extracted from a pretrained model (e.g., EfficientNet [18], ResNet [19], ConvNeXt [20], or ViT [21]) through a two-layer fully connected network with batch normalization, ReLU activation, dropout regularization, and group normalization, mapping inputs to an embedding vector of 512 dimensions. These vectors are subsequently processed by multi-head cross-attention pooling (CAP), implemented using one of three possible attention functions, followed by similarity calculations [4]. The key mechanism here is CAP, which employs cross-attention to use information from

the query vector to adaptively pool the four vectors in the target bag into a single vector. To investigate the effect of using multiple attention heads, we also include a version of the architecture that performs single-head attention-based pooling in our experiments.

As shown in Figure 2, the feature extraction is performed for both query image and a target bag (the number of images used in the target set is 4). This step is followed by using multi-head attention, which extracts representations of the query, yielding a vector  $V_Q$ , and the target set, yielding a vector  $V_T$ . These representations are then used by a Siamese network for the classification task.

### 3.1.1 Different Attention Mechanisms

Variance-excited multi-head attention (VEMA) [4] computes attention scores by gating query vectors through variance-derived transformations of the target set, incorporating learnable projection matrices  $R$  and  $S$  to modulate query representations based on target variance. Distance-based attention (DBA) [4] calculates attention weights using either L1 or L2 distances between query and target embeddings, normalized by learnable beta parameters and theoretical constants derived from the expected distance distributions. DBA is considered a simpler alternative to VEMA [4]. Multi-head squeeze-and-excitation (MHSCE) applies channel-wise recalibration through global average pooling and two fully connected layers, generating excitation vectors that modulate both the attended target representations and original query embeddings. Additionally, as a baseline, we use no-attention mechanisms using mean or max pooling, thus enabling a direct comparison against attention-free aggregation strategies.

### 3.1.2 Training and Hyperparameters

We employ  $k$ -fold cross-validation with patient-level stratification. Each fold is trained for up to 50 epochs using binary cross-entropy loss optimized via RMSprop (in line with [4]) with an initial learning rate of 0.0001, which is reduced using a learning rate scheduler. The training procedure incorporates early stopping (with a patience of 10 epochs) regarding the validation loss, which seeks to identify the optimal model checkpoint and prevent overfitting.

The experiments evaluate multiple architectural configurations by considering a grid over attention types (VEMA, DBA-L1, DBA-L2, no-attention with mean pooling, no-attention with max pooling) and numbers of attention heads ( $h = 1, 2, 4, 8, 16$ ). For each configuration, models are trained across all  $k = 10$  folds, with the best-performing fold model (associated with the least loss) subsequently evaluated on the held-out test set. All predictions utilize a fixed decision threshold of 0.5 (model outputs probabilities are in the range  $[0,1]$ ) for binary classification, ensuring consistent evaluation across configurations and eliminating threshold optimization as a confounding variable.

## 3.2 SimCLR and MIV

In order to investigate whether the performance of the MIV models used in this paper can benefit from a contrastive learning approach. We also consider using simple

framework for contrastive learning of visual representations (SimCLR) [22] to generate embeddings from polyp images from the PillCam data.

We implement a SimCLR architecture consisting of three primary components: a backbone encoder, a projection head, and a contrastive loss function. The backbone encoder utilizes pre-trained deep learning models (EfficientNet [18], ResNet [19], ConvNeXt [20], ViT [21]) to extract high-dimensional feature representations from input images. The projection head is implemented as a two-layer perceptron that transforms these backbone features through a hidden layer of 2048 dimensions before projecting to a final 512-dimensional embedding space. For details, please see Table 1. This projection head incorporates batch normalization and employs ReLU activation. It applies L2 normalization to the final projections, ensuring all embeddings reside on the unit hypersphere, where angular distances effectively capture semantic similarity. The contrastive learning objective is realized through the normalized temperature-scaled cross entropy (NT-Xent) loss [23], which maximizes agreement between differently augmented views of the same image while minimizing agreement with augmented views of other images within the batch.

**Table 1** Details of the models and parameters used for SimCLR experiments. All experiments run 200 epochs and a batch size of 64.

Pretrained base model	Embedding dimension	Projection dimension	Optimizer
ViT	768	512	AdamW
ResNet-50	2048	512	LARS
Efficientnet-B5	2048	512	LARS
ConvNeXt	1024	512	LARS

### 3.2.1 Training SimCLR

The training procedure for the feature extractor based on SimCLR is tailored to the specific characteristics of different backbone architectures. For convolutional neural network backbones, we employ the layer-wise adaptive rate scaling (LARS) [24] optimizer with a base learning rate of 0.3, scaled proportionally to the batch size, combined with minimal weight decay of 1e-6 and momentum of 0.9. For the Vision Transformer backbone, the implementation uses the AdamW optimizer [25] with a lower base learning rate of 3e-4 and stronger regularization through weight decay of 0.05. The learning rate schedule incorporates a warmup strategy [26–28] for 10 epochs, during which the learning rate linearly increases from zero to the base value, followed by cosine annealing decay [28, 29] to a minimum learning rate of 1e-5 over the remaining training duration of up to 200 epochs. Data augmentation applies multiple stochastic transformations including random resized crops, horizontal and vertical flips, rotations, color jittering, random grayscale, and Gaussian blur. Early stopping with patience of 20 epochs is used.

## 4 Results

Based on the results shown in Tables 2, 3, 4, 5, 6, 7, 8, 9, we can observe that the baseline models without attention mechanisms i.e., no attention(mean) and no attention(max) consistently achieve moderate performance across all architectures, with validation accuracies ranging from approximately 75.6% to 81.7% and test accuracies between 74.6% and 82.9%. Similarly, AUC scores on the validation data range from approximately 0.82% to 0.9% and those on the test data range from 0.82% to 0.91%. These baselines establish that both mean and max pooling provide reasonable starting points. Note that neither consistently outperforms the other across different backbone architectures.

Attention mechanisms substantially improved model performance across all tested architectures. VEMA-based configurations demonstrate strong improvements, particularly when using multiple attention heads. For instance, in Tables 2, with the pretrained ResNet-50 backbone, VEMA with 16 heads achieves a test accuracy of 83.55% and test AUC of 0.924, representing significant gains over the no-attention baseline. In a similar manner (in Table 4), we notice that the ViT backbone shows steady improvement from single-head to multi-head configurations, reaching 81.05% test accuracy and test AUC of 0.901 with 16 heads. Similar trends are observed for test accuracies and test AUCs for EfficientNet and ConvNeXt backbones, respectively, as shown in Tables 6, and 8.

The DBA mechanisms, implemented with both L1 and L2 distance metrics, shows competitive and often superior performance compared to VEMA. Notably, DBA consistently achieves better results across different number of attention heads. For the SimCLR framework with ConvNeXt backbone, DBA L1 with 2 heads achieves the highest test accuracy of 86.26% and a test AUC of 0.928. The choice between L1 and L2 distance metrics appears architecture-dependent, with neither consistently dominating across all experiments performed in this paper.

The integration of self-supervised learning through SimCLR pretraining generally enhances performance across architectures. SimCLR-pretrained models often achieved higher validation and test accuracies compared to their standard pretrained counterparts. For example, the EfficientNet backbone with SimCLR pretraining and DBA L1 with 2 heads reaches approx. 84.82% validation accuracy, 83.46% test accuracy and test AUC of 0.926 , outperforming the standard pretrained EfficientNet configuration. This suggests that the learned representations from contrastive learning provide a good foundation for attention-based classification.

Across all tested architectures, the optimal number of attention heads varies, but configurations with 2 to 8 heads frequently yielded the best results. Increasing to 16 heads sometimes improves performance but occasionally leads to slight degradation (see Tables 3 and 8), suggesting that excessive attention capacity may introduce noise or overfitting. The ConvNeXt architecture with SimCLR pretraining achieved the highest overall performance metrics, indicating that modern convolutional architectures combined with self-supervised learning and attention mechanisms represent a particularly effective combination for this classification task.

Figure 3 shows classification output examples for the MIV model using the pretrained ConvNext. Note that the model has a test accuracy of 83.66% for DBA L2

**Table 2** Validation and test performance across different attention mechanisms for pretrained ResNet-50 model. Please note that validation accuracy and validation AUC values (mean  $\pm$  one standard deviation) are based on  $k = 10$  folds.

Experiment	Val Acc (%)	Test Acc (%)	Val AUC	Test AUC
No attention(mean)	79.19 $\pm$ 2.65	77.72	0.871 $\pm$ 0.023	0.852
No attention(max)	78.85 $\pm$ 3.89	79.27	0.863 $\pm$ 0.037	0.881
VEMA(h=1)	79.59 $\pm$ 1.67	76.68	0.866 $\pm$ 0.019	0.851
VEMA(h=2)	82.63 $\pm$ 1.72	82.64	0.890 $\pm$ 0.019	0.897
VEMA(h=4)	82.68 $\pm$ 1.67	82.51	0.892 $\pm$ 0.023	0.902
VEMA(h=8)	82.92 $\pm$ 1.54	80.57	0.896 $\pm$ 0.019	0.897
VEMA(h=16)	83.36 $\pm$ 2.38	83.55	0.898 $\pm$ 0.022	0.924
DBA L1(h=1)	79.14 $\pm$ 2.62	79.15	0.866 $\pm$ 0.034	0.879
DBA L1(h=2)	83.01 $\pm$ 2.96	80.70	0.896 $\pm$ 0.028	0.875
DBA L1(h=4)	83.24 $\pm$ 1.99	82.25	0.900 $\pm$ 0.016	0.886
DBA L1(h=8)	82.28 $\pm$ 2.03	82.38	0.899 $\pm$ 0.021	0.907
DBA L1(h=16)	82.89 $\pm$ 1.88	83.03	0.895 $\pm$ 0.024	0.902
DBA L2(h=1)	79.67 $\pm$ 2.68	78.37	0.868 $\pm$ 0.021	0.871
DBA L2(h=2)	82.71 $\pm$ 2.45	83.16	0.892 $\pm$ 0.028	0.902
DBA L2(h=4)	82.64 $\pm$ 2.20	83.16	0.893 $\pm$ 0.020	0.894
DBA L2(h=8)	83.29 $\pm$ 2.89	82.51	0.902 $\pm$ 0.025	0.902
DBA L2(h=16)	82.92 $\pm$ 2.24	83.55	0.897 $\pm$ 0.019	0.900

with 2 heads. In each row, the leftmost image is the query and the four images to the right of each query are the target images. The True Positive (left-top) and True Negative (bottom-right) examples outline the cases when the model is able to successfully distinguish images containing unique polyps from those with dissimilar polyps. The False Negative (top-right) and False Positive (bottom-left) examples show the cases where the model fails to correctly distinguish images of unique polyps and images of dissimilar polyps. Further, we can note from the differences in the examples of True Positives and False Negatives that when the query image and the target set instances differ from each other in some ways, then the model can misclassify images. These differences could be attributed to different views due to the dynamics of the camera inside the colon, different views from two camera heads of the capsule, or presence of artifacts such as bubbles, debris, and small bowel secretions.

On the other hand, when we look at the examples of False Positives (Pred = true, Label = false) in Figure 3, we can note that if images in the target match the query in ways such as texture, color, illumination conditions, presence of artifacts, then this may lead to misidentification of the query as belonging to the targets. For True Negative (Pred = false, Label = false) examples, we can see that presence of significant differences between the query and the targets leads to correct identification of the image sets as different.

Similarly, we consider examples for the MIV model based on SimCLR pretraining using the pretrained ConvNext backbone in Figure 4. The model has a test accuracy of 86.26% for DBA L1 with 2 heads. Here we note again a similar trend by looking at the True Positive and False Negative examples as observed before, where a significant difference in the query image when compared with the target images can lead to a

**Table 3** Validation and test performance across different attention mechanisms for SimCLR with pretrained ResNet-50 backbone

Experiment	Val Acc (%)	Test Acc (%)	Val AUC	Test AUC
No attention(mean)	79.85 $\pm$ 3.53	80.53	0.883 $\pm$ 0.029	0.886
No attention(max)	80.47 $\pm$ 3.26	78.12	0.884 $\pm$ 0.031	0.879
VEMA(h=1)	80.37 $\pm$ 2.91	81.17	0.884 $\pm$ 0.023	0.896
VEMA(h=2)	84.09 $\pm$ 3.18	83.97	0.901 $\pm$ 0.030	0.910
VEMA(h=4)	84.36 $\pm$ 3.02	83.21	0.899 $\pm$ 0.026	0.891
VEMA(h=8)	83.71 $\pm$ 3.20	83.59	0.899 $\pm$ 0.024	0.895
VEMA(h=16)	82.76 $\pm$ 2.69	84.99	0.900 $\pm$ 0.026	0.915
DBA L1(h=1)	80.09 $\pm$ 3.10	79.77	0.882 $\pm$ 0.027	0.881
DBA L1(h=2)	84.43 $\pm$ 3.05	83.72	0.905 $\pm$ 0.025	0.890
DBA L1(h=4)	83.35 $\pm$ 2.46	84.61	0.898 $\pm$ 0.025	0.925
DBA L1(h=8)	84.44 $\pm$ 2.73	84.61	0.908 $\pm$ 0.022	0.915
DBA L1(h=16)	83.69 $\pm$ 2.71	82.95	0.904 $\pm$ 0.024	0.908
DBA L2(h=1)	79.91 $\pm$ 2.81	80.79	0.885 $\pm$ 0.026	0.903
DBA L2(h=2)	85.20 $\pm$ 2.90	84.10	0.900 $\pm$ 0.029	0.899
DBA L2(h=4)	84.15 $\pm$ 3.17	83.72	0.909 $\pm$ 0.025	0.904
DBA L2(h=8)	84.28 $\pm$ 2.66	84.99	0.906 $\pm$ 0.023	0.917
DBA L2(h=16)	83.29 $\pm$ 3.19	83.72	0.911 $\pm$ 0.024	0.923

**Table 4** Validation and test performance across different attention mechanisms for pretrained ViT backbone

Experiment	Val Acc (%)	Test Acc (%)	Val AUC	Test AUC
No attention(mean)	76.74 $\pm$ 2.46	74.65	0.838 $\pm$ 0.023	0.819
No attention(max)	77.24 $\pm$ 3.34	75.42	0.847 $\pm$ 0.029	0.835
VEMA(h=1)	77.21 $\pm$ 2.53	77.72	0.844 $\pm$ 0.028	0.856
VEMA(h=2)	80.14 $\pm$ 3.42	78.49	0.875 $\pm$ 0.021	0.853
VEMA(h=4)	81.46 $\pm$ 2.42	80.03	0.898 $\pm$ 0.018	0.877
VEMA(h=8)	81.71 $\pm$ 2.43	80.92	0.889 $\pm$ 0.012	0.890
VEMA(h=16)	81.14 $\pm$ 2.47	80.92	0.896 $\pm$ 0.018	0.891
DBA L1(h=1)	76.94 $\pm$ 1.99	75.80	0.837 $\pm$ 0.022	0.822
DBA L1(h=2)	81.93 $\pm$ 2.22	79.13	0.886 $\pm$ 0.017	0.864
DBA L1(h=4)	81.81 $\pm$ 2.65	80.79	0.896 $\pm$ 0.015	0.888
DBA L1(h=8)	80.89 $\pm$ 2.92	80.41	0.891 $\pm$ 0.019	0.886
DBA L1(h=16)	81.49 $\pm$ 2.51	81.05	0.900 $\pm$ 0.020	0.901
DBA L2(h=1)	76.74 $\pm$ 2.68	77.46	0.841 $\pm$ 0.028	0.846
DBA L2(h=2)	81.72 $\pm$ 2.79	80.15	0.893 $\pm$ 0.018	0.889
DBA L2(h=4)	81.82 $\pm$ 2.54	78.87	0.893 $\pm$ 0.016	0.866
DBA L2(h=8)	81.90 $\pm$ 2.31	76.95	0.891 $\pm$ 0.019	0.863
DBA L2(h=16)	81.25 $\pm$ 2.88	78.87	0.894 $\pm$ 0.018	0.884

failure to identify the same polyp images in the five examples. A look at the False Positive examples affirms that the task remains challenging, as evidenced by the model’s occasional misclassifications in ambiguous cases.

We can additionally consider the confusion matrices from the best MIV model associated with (a) the pretrained ConvNext and (b) SimCLR pretraining using the ConvNext backbone in Figure 4. We note that using SimCLR achieves a better ratio

**Table 5** Comparison of validation and test performance across different attention mechanisms for SimCLR using ViT pretrained backbone

Experiment	Val Acc (%)	Test Acc (%)	Val AUC	Test AUC
No attention(mean)	78.49 $\pm$ 3.47	80.92	0.861 $\pm$ 0.026	0.882
No attention(max)	76.32 $\pm$ 2.96	81.17	0.856 $\pm$ 0.028	0.879
VEMA(h=1)	77.94 $\pm$ 3.46	75.83	0.865 $\pm$ 0.030	0.852
VEMA(h=2)	81.64 $\pm$ 2.66	80.03	0.896 $\pm$ 0.031	0.899
VEMA(h=4)	<u>83.00<math>\pm</math>1.96</u>	80.41	0.905 $\pm$ 0.016	0.886
VEMA(h=8)	81.75 $\pm$ 2.71	82.57	<u>0.909<math>\pm</math>0.015</u>	0.910
VEMA(h=16)	81.66 $\pm$ 2.87	82.44	0.904 $\pm$ 0.025	<u>0.914</u>
DBA L1(h=1)	76.82 $\pm$ 2.75	78.12	0.857 $\pm$ 0.025	0.858
DBA L1(h=2)	82.13 $\pm$ 2.41	82.06	<u>0.909<math>\pm</math>0.020</u>	0.896
DBA L1(h=4)	82.16 $\pm$ 2.96	78.88	0.904 $\pm$ 0.022	0.874
DBA L1(h=8)	82.27 $\pm$ 2.74	80.79	0.904 $\pm$ 0.017	0.883
DBA L1(h=16)	81.80 $\pm$ 3.18	79.52	0.904 $\pm$ 0.022	0.895
DBA L2(h=1)	77.10 $\pm$ 3.62	79.39	0.853 $\pm$ 0.032	0.844
DBA L2(h=2)	81.78 $\pm$ 2.00	79.01	0.892 $\pm$ 0.028	0.854
DBA L2(h=4)	81.90 $\pm$ 2.34	<u>83.72</u>	0.903 $\pm$ 0.018	0.896
DBA L2(h=8)	81.03 $\pm$ 2.49	80.92	0.899 $\pm$ 0.025	0.877
DBA L2(h=16)	82.31 $\pm$ 2.28	82.57	0.907 $\pm$ 0.020	0.910

**Table 6** Comparison of validation and test performance across different attention mechanisms for pretrained EfficientNet

Experiment	Val Acc (%)	Test Acc (%)	Val AUC	Test AUC
No attention(mean)	76.32 $\pm$ 3.35	76.19	0.845 $\pm$ 0.031	0.845
No attention(max)	75.63 $\pm$ 2.57	76.59	0.842 $\pm$ 0.021	0.855
VEMA(h=1)	77.07 $\pm$ 2.96	76.19	0.845 $\pm$ 0.030	0.844
VEMA(h=2)	81.19 $\pm$ 1.74	78.70	0.886 $\pm$ 0.024	0.891
VEMA(h=4)	81.23 $\pm$ 3.19	<u>81.88</u>	0.882 $\pm$ 0.029	<u>0.906</u>
VEMA(h=8)	81.79 $\pm$ 3.32	78.70	0.893 $\pm$ 0.023	0.864
VEMA(h=16)	81.57 $\pm$ 3.07	80.42	0.894 $\pm$ 0.022	0.883
DBA L1(h=1)	76.48 $\pm$ 3.66	76.06	0.838 $\pm$ 0.031	0.844
DBA L1(h=2)	81.75 $\pm$ 2.91	79.76	0.890 $\pm$ 0.029	0.885
DBA L1(h=4)	<u>81.90<math>\pm</math>2.48</u>	80.29	0.888 $\pm$ 0.024	0.867
DBA L1(h=8)	82.01 $\pm$ 2.72	78.04	0.891 $\pm$ 0.018	0.859
DBA L1(h=16)	81.30 $\pm$ 1.89	79.89	<u>0.893<math>\pm</math>0.024</u>	0.877
DBA L2(h=1)	76.57 $\pm$ 2.35	79.50	0.841 $\pm$ 0.023	0.870
DBA L2(h=2)	80.22 $\pm$ 3.54	77.78	0.871 $\pm$ 0.025	0.868
DBA L2(h=4)	81.40 $\pm$ 3.62	79.76	0.882 $\pm$ 0.034	0.877
DBA L2(h=8)	81.41 $\pm$ 2.43	79.23	0.886 $\pm$ 0.026	0.863
DBA L2(h=16)	81.15 $\pm$ 2.97	80.82	0.889 $\pm$ 0.031	0.858

of False Negatives (70) to False Positives (38) as compared to pretrained ConvNext, which has 109 False Negatives and 23 False Positives.

**Table 7** Comparison of validation and test performance across different attention mechanisms using SimCLR and pretrained Efficientnet as backbone

Experiment	Val Acc (%)	Test Acc (%)	Val AUC	Test AUC
No attention(mean)	79.01 $\pm$ 3.99	81.42	0.874 $\pm$ 0.029	0.900
No attention(max)	80.11 $\pm$ 3.21	80.66	0.876 $\pm$ 0.028	0.886
VEMA(h=1)	80.15 $\pm$ 3.57	79.90	0.880 $\pm$ 0.030	0.899
VEMA(h=2)	83.53 $\pm$ 2.81	82.57	0.902 $\pm$ 0.034	0.901
VEMA(h=4)	83.99 $\pm$ 3.18	81.68	0.899 $\pm$ 0.027	0.890
VEMA(h=8)	83.30 $\pm$ 2.99	83.33	0.901 $\pm$ 0.024	0.894
VEMA(h=16)	82.75 $\pm$ 3.46	79.64	0.907 $\pm$ 0.026	0.883
DBA L1(h=1)	80.49 $\pm$ 2.67	80.66	0.882 $\pm$ 0.027	0.888
DBA L1(h=2)	84.82 $\pm$ 2.22	83.46	0.903 $\pm$ 0.024	0.926
DBA L1(h=4)	83.63 $\pm$ 2.97	82.44	0.896 $\pm$ 0.029	0.885
DBA L1(h=8)	84.01 $\pm$ 2.97	80.92	0.901 $\pm$ 0.028	0.900
DBA L1(h=16)	83.12 $\pm$ 2.74	83.84	0.901 $\pm$ 0.027	0.925
DBA L2(h=1)	79.49 $\pm$ 3.06	80.28	0.876 $\pm$ 0.030	0.878
DBA L2(h=2)	83.46 $\pm$ 2.59	83.72	0.897 $\pm$ 0.028	0.906
DBA L2(h=4)	83.71 $\pm$ 3.20	83.97	0.900 $\pm$ 0.022	0.910
DBA L2(h=8)	84.82 $\pm$ 3.01	81.55	0.911 $\pm$ 0.022	0.894
DBA L2(h=16)	83.58 $\pm$ 2.17	82.06	0.907 $\pm$ 0.021	0.892

**Table 8** Comparison of validation and test performance across different attention mechanisms for pretrained ConvNeXt

Experiment	Val Acc (%)	Test Acc (%)	Val AUC	Test AUC
No attention(mean)	79.99 $\pm$ 2.55	81.68	0.879 $\pm$ 0.026	0.895
No attention(max)	79.64 $\pm$ 2.35	80.07	0.878 $\pm$ 0.018	0.887
VEMA(h=1)	80.43 $\pm$ 3.06	81.81	0.885 $\pm$ 0.019	0.888
VEMA(h=2)	82.30 $\pm$ 2.00	82.05	0.898 $\pm$ 0.024	0.901
VEMA(h=4)	82.72 $\pm$ 2.10	83.29	0.904 $\pm$ 0.016	0.903
VEMA(h=8)	83.44 $\pm$ 2.55	82.43	0.902 $\pm$ 0.024	0.890
VEMA(h=16)	82.81 $\pm$ 2.17	83.29	0.906 $\pm$ 0.016	0.894
DBA L1(h=1)	80.06 $\pm$ 3.26	80.32	0.876 $\pm$ 0.019	0.886
DBA L1(h=2)	83.22 $\pm$ 2.23	82.80	0.903 $\pm$ 0.017	0.887
DBA L1(h=4)	83.25 $\pm$ 2.19	83.29	0.909 $\pm$ 0.019	0.901
DBA L1(h=8)	82.26 $\pm$ 1.90	81.06	0.891 $\pm$ 0.021	0.896
DBA L1(h=16)	83.24 $\pm$ 2.61	82.05	0.910 $\pm$ 0.021	0.901
DBA L2(h=1)	80.86 $\pm$ 2.97	81.68	0.886 $\pm$ 0.019	0.894
DBA L2(h=2)	82.53 $\pm$ 2.56	83.66	0.895 $\pm$ 0.029	0.913
DBA L2(h=4)	83.18 $\pm$ 1.74	81.68	0.900 $\pm$ 0.020	0.889
DBA L2(h=8)	83.04 $\pm$ 1.83	83.04	0.895 $\pm$ 0.020	0.894
DBA L2(h=16)	82.88 $\pm$ 1.97	81.31	0.905 $\pm$ 0.015	0.904

#### 4.1 Discussion

Based on the results presented in the study, the proposed Multi-Instance Learning (MIL) framework demonstrates significant potential in addressing the challenge of identifying unique polyps in CCE images. The integration of attention mechanisms, particularly Distance-Based Attention (DBA) and Variance-Excited Multi-head

**Table 9** Comparison of validation and test performance across different attention mechanisms for SimCLR using pretrained ConvNeXt backbone

Experiment	Val Acc (%)	Test Acc (%)	Val AUC	Test AUC
No attention(mean)	81.63 $\pm$ 3.84	82.95	0.900 $\pm$ 0.027	0.910
No attention(max)	81.69 $\pm$ 2.51	81.55	0.899 $\pm$ 0.021	0.911
VEMA(h=1)	81.20 $\pm$ 2.99	81.93	0.897 $\pm$ 0.020	0.897
VEMA(h=2)	<u>85.86<math>\pm</math>3.05</u>	82.32	<u>0.915<math>\pm</math>0.028</u>	0.882
VEMA(h=4)	84.84 $\pm$ 2.80	83.33	0.911 $\pm$ 0.028	0.908
VEMA(h=8)	84.13 $\pm$ 3.09	84.10	0.907 $\pm$ 0.026	0.913
VEMA(h=16)	83.63 $\pm$ 3.67	83.46	0.907 $\pm$ 0.025	0.901
DBA L1(h=1)	81.68 $\pm$ 3.14	81.55	0.896 $\pm$ 0.016	0.904
DBA L1(h=2)	84.54 $\pm$ 3.19	<u>86.26</u>	0.914 $\pm$ 0.021	<u>0.928</u>
DBA L1(h=4)	84.98 $\pm$ 2.73	85.24	0.910 $\pm$ 0.027	0.907
DBA L1(h=8)	84.75 $\pm$ 2.77	83.46	0.913 $\pm$ 0.024	0.920
DBA L1(h=16)	84.39 $\pm$ 2.78	83.08	0.911 $\pm$ 0.021	0.903
DBA L2(h=1)	82.07 $\pm$ 3.36	83.08	0.901 $\pm$ 0.020	0.911
DBA L2(h=2)	85.66 $\pm$ 3.29	84.48	0.914 $\pm$ 0.030	0.922
DBA L2(h=4)	84.99 $\pm$ 3.63	83.33	0.913 $\pm$ 0.032	0.920
DBA L2(h=8)	83.99 $\pm$ 3.14	84.10	0.912 $\pm$ 0.025	0.904
DBA L2(h=16)	84.11 $\pm$ 2.46	84.10	0.909 $\pm$ 0.022	0.908

Attention (VEMA), has shown to enhance the model’s ability to extract useful representations, leading to improved classification performance. Notably, the DBA L1 mechanism with SimCLR pretraining achieved the highest test accuracy of 86.26% and a test AUC of 0.928, underscoring the efficacy of combining self-supervised learning with attention-based MIL frameworks. However, the analysis of misclassifications of positive examples (False Negatives) reveals that the task remains challenging, particularly in cases where the query and target images exhibit significant differences. On the other hand, in case of False Positives, we note that the presence of similar structures (texture, color, or artifacts) between the query image and target bag can lead to misidentification of different polyp images as belonging to the same polyp.

The misclassifications (False Negatives and False Positives) in MIV models can be attributed to first, the fact that the dataset is limited to 1912 unique polyps from 754 patients and both, studies and data, within this specific subdomain are lacking. The MIV models can struggle to classify images that differ significantly from those seen during the training phase. Second, the PillCam capsule with its two-headed camera can capture different views of a polyp sometimes from opposite directions hence making the task of identifying unique polyps quite challenging.

To alleviate the challenges of a lack of data, use of synthetic data generation as discussed in [30] for CCE images can be seen as the next step to address the challenges of limited data with labels. However, according to the authors, it is important to note that synthetic images can have unrealistic appearance of anatomical structures [30].

We believe that our proposed methodology can be extended to other diagnoses (e.g., ulcers, bleeding, diverticula, and inflammatory bowel disease) [31, 32] within CCE and even domains beyond CCE, where large datasets with limited or weakly labeled instances are common. By replacing the reliance on extensive manual annotations to annotations at bag level, this work paves the way for more efficient, accurate,

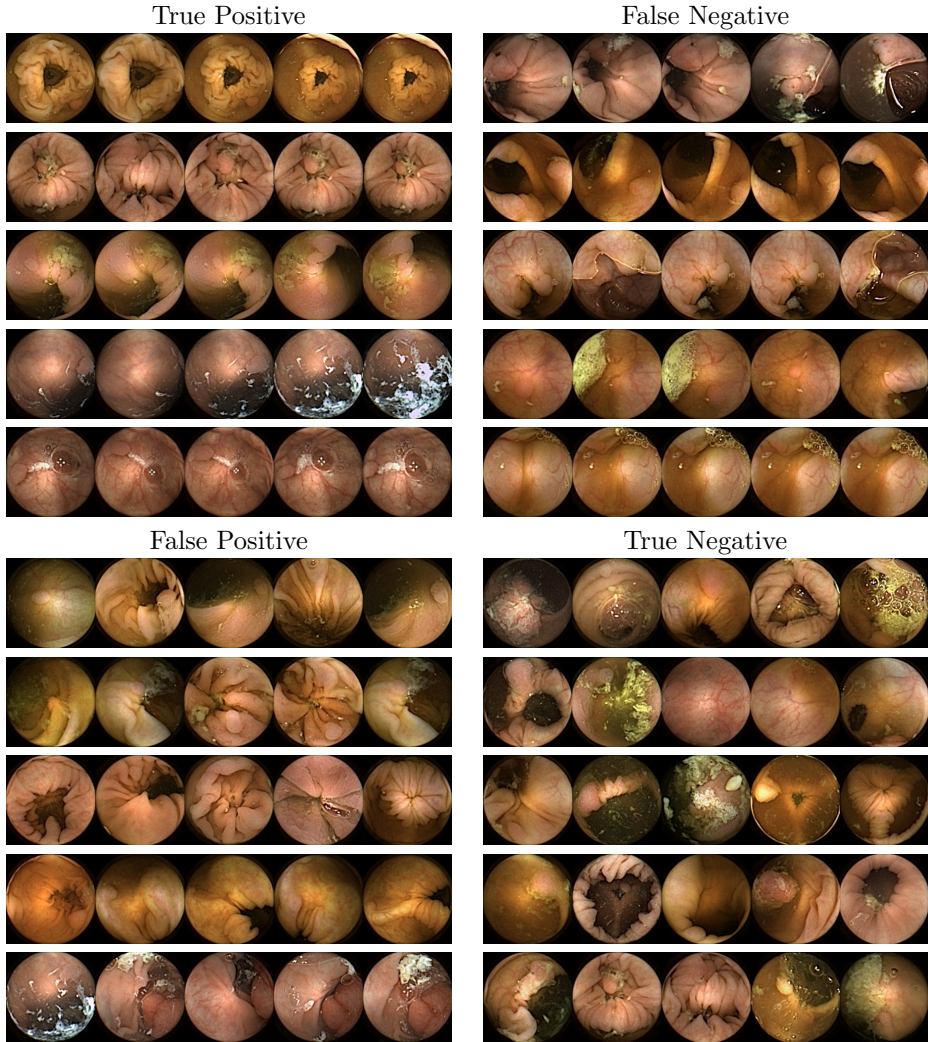


**Fig. 3** True Positives (Pred = true, Label = true), False Negatives (Pred = false, Label = true), False Positives (Pred = true, Label = false), True Negatives (Pred = false, Label = false) for the DBA L2(h=2) model using the pretrained ConvNeXt. In each row, the leftmost image is the query and the 4 images to the right of each query are the target images.

and scalable diagnostic tools. Ultimately, these advancements can contribute to reducing clinician workload, improving diagnostic accuracy, thereby enhancing patient outcomes and advancing the broader field of medical imaging and AI.

## 5 Conclusions

In this paper, we formulate the problem of identifying unique polyps in CCE images as a multi-instance learning problem where a query polyp image is compared with a target

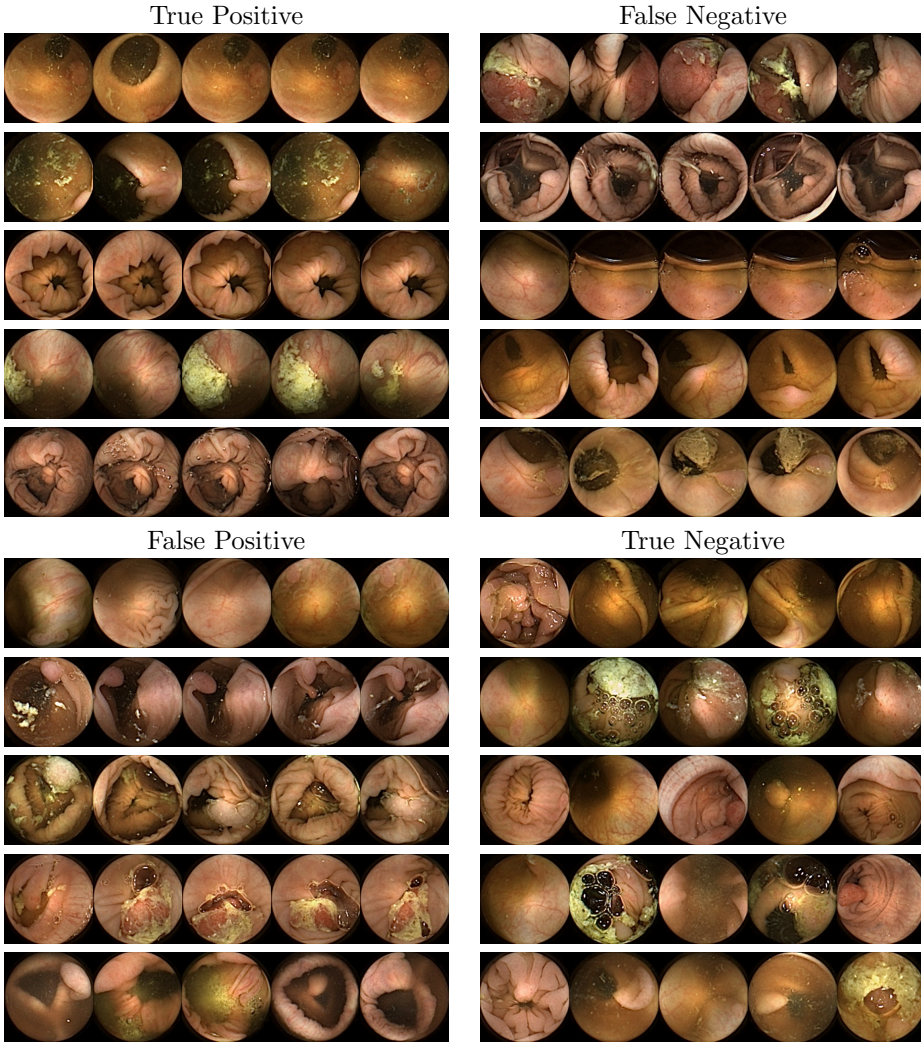


**Fig. 4** True Positives (Pred = true, Label = true), False Negatives (Pred = false, Label = true), False Positives (Pred = true, Label = false), True Negatives (Pred = false, Label = false) for the DBA L1(h=2) model applying SimCLR using the ConvNeXt backbone. In each row, the leftmost image is the query and the 4 images to the right of each query are the target images.

bag of images. Baseline models without attention mechanisms, utilizing mean or max pooling strategies, achieve moderate performance, with validation accuracies ranging from 76.3% to 81.7% and test accuracies between 74.2% and 82.9%. The inclusion of attention mechanisms, such as VEMA and Distance-Based Attention (DBA), lead to substantial improvements. VEMA shows strong gains, particularly with multi-head configurations, while DBA mechanisms, leveraging L1 and L2 distance metrics, often outperform VEMA and achieve competitive results across architectures. Notably, DBA L1 with 2 heads achieves the highest test accuracy of 86.26% and a test AUC of 0.928

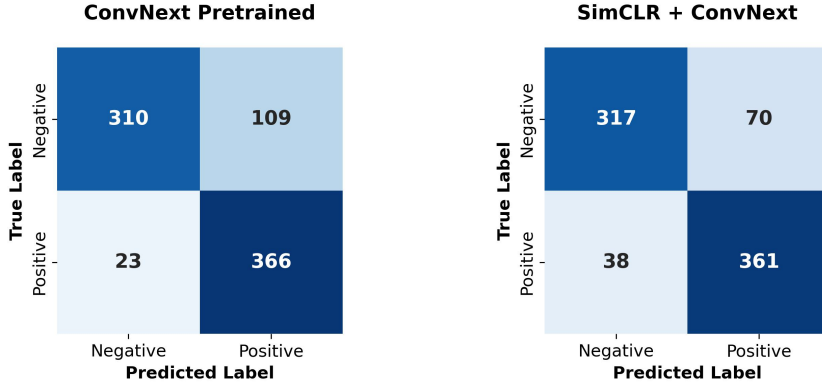


**Fig. 5** Confusion matrices from the best MIV model associated with (left) the pretrained ConvNext, and (right) SimCLR pretraining using the ConvNext backbone

using the ConvNeXt backbone with SimCLR pretraining. SimCLR pretraining further enhances performance, with models pretrained using SimCLR consistently achieving higher validation and test accuracies compared to standard pretrained counterparts. Despite these advancements, challenges remain in distinguishing between images of unique polyps and dissimilar polyps, particularly in edge cases where query images and target instances differ, underscoring the complexity of the classification task.

## Acknowledgment

This research is part of AICE project (number 101057400) funded by the European Union, and it is part-funded by the United Kingdom government. Views and opinions expressed are however those of the author(s) only and do not necessarily reflect those of the European Union or the European Commission. Neither the European Union nor the European Commission can be held responsible for them.



## References

- [1] Dietterich, T.G., Lathrop, R.H., Lozano-Pérez, T.: Solving the multiple instance problem with axis-parallel rectangles. *Artificial Intelligence* **89**(1), 31–71 (1997) [https://doi.org/10.1016/S0004-3702\(96\)00034-3](https://doi.org/10.1016/S0004-3702(96)00034-3)
- [2] Maron, O., Lozano-Pérez, T.: A framework for multiple-instance learning. In: Jordan, M., Kearns, M., Solla, S. (eds.) *Proceedings of the 11th International Conference on Neural Information Processing Systems*, pp. 570–576 (1997). MIT Press

- [3] Ilse, M., Tomczak, J., Welling, M.: Attention-based deep multiple instance learning. In: International Conference on Machine Learning, pp. 2127–2136 (2018). PMLR
- [4] Xu, X., Frank, E., Holmes, G.: Multiple instance verification. *Journal of Machine Learning Research* **26**(188), 1–46 (2025)
- [5] Spada, C., Hassan, C., Campanale, M., Costamagna, G.: Colon capsule endoscopy. *Techniques in Gastrointestinal Endoscopy* **17**(1), 19–23 (2015)
- [6] Eliakim, R., Yassin, K., Niv, Y., Metzger, Y., Lachter, J., Gal, E., Sapoznikov, B., Konikoff, F., Leichtmann, G., Fireman, Z., Kopelman, Y., Adler, N.S.: Prospective multicenter performance evaluation of the second-generation colon capsule compared with colonoscopy. *Endoscopy* **41**(12), 1026–1031 (2009)
- [7] Pasha, S.F.: Applications of colon capsule endoscopy. *Current gastroenterology reports* **20**(5), 22 (2018)
- [8] Eliakim, R., Fireman, Z., Gralnek, I.M., Yassin, K., Waterman, M., Kopelman, Y., Lachter, J., Koslowsky, B., Adler, S.N.: Evaluation of the pillcam colon capsule in the detection of colonic pathology: results of the first multicenter, prospective, comparative study. *Endoscopy* **38**(10), 963–970 (2006)
- [9] Hosoe, N., Limpias Kamiya, K.J., Hayashi, Y., Sujino, T., Ogata, H., Kanai, T.: Current status of colon capsule endoscopy. *Digestive Endoscopy* **33**(4), 529–537 (2021)
- [10] Spada, C., Hassan, C., Munoz-Navas, M., Neuhaus, H., Deviere, J., Fockens, P., Coron, E., Gay, G., Toth, E., Riccioni, M.E., Carretero, C., Charton, J.P., Gossum, A.V., Wientjes, C.A., Sacher-Huvelin, S., Delvaux, M., Nemeth, A., Petruzziello, L., Frias, C.P., Mayershofer, R., Aminejab, L., Dekker, E., Galmiche, J.-P., Frederic, M., Johansson, G.W., Cesaro, P., Costamagna, G.: Second-generation colon capsule endoscopy compared with colonoscopy. *Gastrointestinal endoscopy* **74**(3), 581–589 (2011)
- [11] Quellec, G., Cazuguel, G., Cochener, B., Lamard, M.: Multiple-instance learning for medical image and video analysis. *IEEE Reviews in Biomedical Engineering* **10**, 213–234 (2017) <https://doi.org/10.1109/RBME.2017.2651164>
- [12] Schlegl, T., Waldstein, S.M., Vogl, W.-D., Schmidt-Erfurth, U., Langs, G.: Predicting semantic descriptions from medical images with convolutional neural networks. In: International Conference on Information Processing in Medical Imaging, pp. 437–448 (2015). Springer
- [13] Li, C., Shi, C., Zhang, H., Chen, Y., Zhang, S.: Multiple instance learning for computer aided detection and diagnosis of gastric cancer with dual-energy CT imaging. *Journal of Biomedical Informatics* **57**, 358–368 (2015) <https://doi.org/>

- [14] Zhao, D., Chen, Y., Correa, H.: Automated classification of human histological images, a multiple-instance learning approach. In: 2006 IEEE/NLM Life Science Systems and Applications Workshop, pp. 1–2 (2006). <https://doi.org/10.1109/LSSA.2006.250411>
- [15] Kaalby, L., Deding, U., Kobaek-Larsen, M., Havshoi, A.-L.V., Zimmermann-Nielsen, E., Thygesen, M.K., Kroijer, R., Bjørsum-Meyer, T., Baatrup, G.: Colon capsule endoscopy in colorectal cancer screening: a randomised controlled trial. *BMJ Open Gastroenterology* **7**(1) (2020)
- [16] Baatrup, G., Bjørsum-Meyer, T., Kaalby, L., Schelde-Olesen, B., Kobaek-Larsen, M., Koulaouzidis, A., Kroijer, R., Al-Najami, I., Buch, N., Høgh, A., Qvist, N., Thygesen, M., Deding, U.: Choice of colon capsule or colonoscopy versus default colonoscopy in fit positive patients in the danish screening programme: a parallel group randomised controlled trial. *Gut* **74**(10), 1–10 (2025) <https://doi.org/10.1136/gutjnl-2024-333687>
- [17] Negreanu, L., Babiuc, R., Bengus, A., Sadagurschi, R.: Pillcam colon 2 capsule in patients unable or unwilling to undergo colonoscopy. *World journal of gastrointestinal endoscopy* **5**(11), 559–567 (2013) <https://doi.org/10.4253/wjge.v5.i11.559>
- [18] Tan, M., Le, Q.: EfficientNet: Rethinking model scaling for convolutional neural networks. In: Chaudhuri, K., Salakhutdinov, R. (eds.) *Proceedings of the 36th International Conference on Machine Learning. Proceedings of Machine Learning Research*, vol. 97, pp. 6105–6114 (2019). PMLR. <https://proceedings.mlr.press/v97/tan19a.html>
- [19] He, K., Zhang, X., Ren, S., Sun, J.: Deep residual learning for image recognition. In: *Proceedings of the IEEE Conference on Computer Vision and Pattern Recognition*, pp. 770–778 (2016)
- [20] Liu, Z., Mao, H., Wu, C.-Y., Feichtenhofer, C., Darrell, T., Xie, S.: A convnet for the 2020s. In: *Proceedings of the IEEE/CVF Conference on Computer Vision and Pattern Recognition*, pp. 11976–11986 (2022)
- [21] Dosovitskiy, A.: An image is worth 16x16 words: Transformers for image recognition at scale. *arXiv preprint arXiv:2010.11929* (2020)
- [22] Chen, T., Kornblith, S., Norouzi, M., Hinton, G.: A simple framework for contrastive learning of visual representations. In: *International Conference on Machine Learning*, pp. 1597–1607 (2020). PMLR
- [23] Robinson, J., Chuang, C.-Y., Sra, S., Jegelka, S.: Contrastive learning with hard negative samples. *arXiv preprint arXiv:2010.04592* (2020)

- [24] You, Y., Zhang, Z., Hsieh, C.-J., Demmel, J., Keutzer, K.: ImageNet training in minutes. In: Proceedings of the 47th International Conference on Parallel Processing, pp. 1–10 (2018)
- [25] Loshchilov, I., Hutter, F.: Decoupled weight decay regularization. arXiv preprint arXiv:1711.05101 (2017)
- [26] Goyal, P., Dollár, P., Girshick, R., Noordhuis, P., Wesolowski, L., Kyrola, A., Tulloch, A., Jia, Y., He, K.: Accurate, large minibatch SGD: Training ImageNet in 1 hour. arXiv preprint arXiv:1706.02677 (2017)
- [27] Vaswani, A., Shazeer, N., Parmar, N., Uszkoreit, J., Jones, L., Gomez, A.N., Kaiser, L., Polosukhin, I.: Attention is all you need. Advances in neural information processing systems **30** (2017)
- [28] He, T., Zhang, Z., Zhang, H., Zhang, Z., Xie, J., Li, M.: Bag of tricks for image classification with convolutional neural networks. In: Proceedings of the IEEE/CVF Conference on Computer Vision and Pattern Recognition (CVPR) (2019)
- [29] Loshchilov, I., Hutter, F.: SGDR: Stochastic gradient descent with warm restarts. arXiv preprint arXiv:1608.03983 (2016)
- [30] Gatoula, P., Diamantis, D.E., Koulaouzidis, A., Carretero, C., Chetcuti-Zammit, S., Valdivia, P.C., González-Suárez, B., Mussetto, A., Plevris, J., Robertson, A., Rosa, B., Toth, E., Iakovidis, D.K.: Clinical evaluation of medical image synthesis: a case study in wireless capsule endoscopy. Scientific Reports **15**(1), 35068 (2025)
- [31] Hosoe, N., Hayashi, Y., Ogata, H.: Colon capsule endoscopy for inflammatory bowel disease. Clinical Endoscopy **53**(5), 550–554 (2020)
- [32] Thorndal, C., Schelde-Olesen, B., Kaalby, L., Deding, U., Thygesen, M.M., Depont, R., Hansen, L.Ø., Andersen, P.V., Baatrup, G., Koulaouzidis, A., Bjørsum-Meyer, T.: Colon capsule endoscopy compared with conventional colonoscopy in patients with colonic diverticulitis: a randomized controlled superiority trial on patient-reported outcomes. Endoscopy (2025)